Author/s:
Yang, K;Tang, WT;Liu, SH;Pandy, MG

Title:
Muscle Contributions to Take-Off Velocity in the Long Jump

Date:
2023-08-01

Citation:
Yang, K., Tang, W. T., Liu, S. H. & Pandy, M. G. (2023). Muscle Contributions to Take-Off Velocity in the Long Jump. Medicine and Science in Sports and Exercise, 55 (8), pp.1434-1444. https://doi.org/10.1249/MSS.0000000000003175.

# MUSCLE CONTRIBUTIONS TO TAKE-OFF VELOCITY IN THE LONG JUMP

Kaiwen Yang[1], Wen-Tzu Tang[2], Shu-Hua Liu[2,3], Marcus G. Pandy[1]

[1]Dept of Mechanical Engineering, University of Melbourne, Parkville, Victoria, Australia

[2]Graduate Institute of Athletics and Coaching Science, National Taiwan Sport University, Taoyuan City, Taiwan

[3]Physical Education Office, Ming Chuan University, Taoyuan City, Taiwan

**REVISION**

Submitted as an original article to Medicine and Science in Sports and Exercise

9 March 2023

Corresponding author:

Marcus G. Pandy, Ph.D.

Dept of Mechanical Engineering

University of Melbourne, Parkville, Victoria, 3010, Australia

Tel: +61 8344 4054; Email: pandym@unimelb.edu.au

## ABSTRACT

**Purpose:** A key determinant of long jump performance is the ability to increase the vertical velocity of the center of mass (COM) while minimizing the loss in forward velocity (running speed) during the take-off phase, but exactly how this occurs is not fully understood. We combined a three-dimensional musculoskeletal model of the body with dynamic optimization theory to simulate the biomechanics of the long jump take-off and determine the contributions of the individual leg muscles to jump performance. **Methods:** The body was modelled as a 29-degree-of-freedom skeleton actuated by a combination of muscles and net joint torques. A dynamic optimization problem was solved to reproduce full-body motion and ground-force data recorded from experienced sub-elite jumpers. The optimization solution then was analyzed to determine each muscle's contribution to the ground-force impulse and hence the change in velocity of the COM during the take-off phase. **Results:** The hip, knee and ankle extensors dominated the change in velocity of the COM during take-off. VAS generated the highest support impulse and contributed one-third (33%) of the increase in vertical COM velocity generated by all the muscles. SOL and GMAX also developed substantial support impulses and contributed 24% and 16% of the increase in vertical COM velocity, respectively. VAS also generated the highest braking impulse and contributed approximately one-half (55%) of the loss in forward COM velocity generated by all the muscles, while SOL and GMAX made much smaller contributions (12% and 7%, respectively). **Conclusions:** VAS, SOL, and GMAX contributed nearly three-quarters (73%) of the increase in vertical COM velocity at take-off, suggesting that these muscles ought to be prioritized in strength training programs aimed at improving long jump performance.


Keywords: sprinting, impulse, muscle training, quadriceps, gluteal, ankle plantarflexors

## INTRODUCTION

Elite long jumpers run up at fast speeds, lower their centers of mass in the last few strides, and plant their legs at relatively steep angles to the ground to propel their bodies as far as possible (1, 2). There are four distinct phases of the long jump – approach, take-off, flight, and landing – but the take-off phase, defined as the period from touchdown to take-off, is thought to be the most critical (3-5). A key determinant of jump performance is the ability to increase the vertical velocity of the center of mass (COM) while minimizing the loss in forward velocity during the take-off phase, but exactly how this happens is not fully understood, primarily because there is no information on how the leg muscles generate the required ground force impulse and change in velocity of the COM.

Many investigators have measured the kinematic and kinetic patterns used by elite and sub-elite athletes to produce a successful long jump (1, 3-6). Hay (1) reported that elite male long jumpers reach speeds slightly higher than 10 m/s four strides before take-off. During the last four strides they also lower their COMs by approximately 10 cm relative to the approach height to lengthen the vertical path over which the body is accelerated, thus increasing the vertical velocity of the COM at take-off (1). From touchdown to take-off, vertical velocity is increased by 3-4 m/s while forward velocity is reduced by 1-2 m/s (3). The corresponding force transmitted to the leg during take-off can be remarkably high: during the initial impact the peak vertical ground reaction force is around 11 times body weight (BW) whereas the peak fore-aft braking force reaches ~4.5 BW (7).

Lees and co-workers (4-6) proposed a mechanism which they called the ‘pivot’ to explain the observed increase in vertical velocity of the COM during take-off. They reasoned that an upward velocity is generated at the expense of forward velocity because the body pivots about a stationary foot after touchdown in much the same way as an inverted pendulum pivots about

a fixed support. Dapena and Chung (8) used a kinematic model of the take-off phase of the high jump that may also be relevant to the long jump. They explained that radial motion of the COM toward the stationary foot after touchdown allows the jumper to increase the vertical velocity of the COM by generating a higher vertical ground reaction force and therefore a higher ground force impulse. Alexander (2) and later Seyfarth et al. (9, 10) developed simple muscle-actuated computational models to simulate the long jump take-off. Alexander (2) found that the longest jump is achieved at the highest run-up speed with the leg set down at an angle of 70$^{o}$ relative to the ground, while Seyfarth et al. (10) showed that the necessary increase in vertical velocity could be generated by rapid stretching (eccentric contractions) of the knee extensor muscles during take-off. An important limitation of these models is that they were unable to reproduce the first peak in the vertical ground reaction force generated during the initial impact. Taking an entirely different approach, Graham-Smith and Lees (5) used multivariate regression analyses to show that the vertical COM velocity during take-off increases with a more extended knee and a lower peak knee flexion velocity at touch-down, whereas the loss in forward COM velocity is minimized by reducing hip adduction and increasing hip extension.

Few studies have recorded muscle electromyographic (EMG) activity during the long jump take-off. Kakihana and Suzuki (11) used kinematic, kinetic, and muscle EMG data to explain the different techniques used by two elite jumpers in terms of the coordinated actions of their leg muscles. They found that higher levels of activity in the hip and knee extensors during the first half of the take-off phase correlated with an increase in the vertical velocity of the COM and the distance jumped. No study to our knowledge has described how the individual leg muscles generate the observed changes in vertical and forward velocities of the COM during the take-off phase.

The main aim of the present study was to determine the contributions of the individual lower-limb muscles to performance of the long jump (jump distance). We combined a three-dimensional musculoskeletal model of the body with dynamic optimization theory to determine the contributions of the individual leg muscles to the ground force impulse and change in velocity of the COM during the take-off phase. Our specific aims were to (1) simulate the biomechanics of the long jump take-off by accurately reproducing full-body motion and ground reaction force data recorded from experienced sub-elite jumpers; and (2) identify those muscles responsible for generating the observed increase in vertical velocity of the COM and the concomitant loss in forward velocity during the take-off phase. A comprehensive understanding of the functional roles of the individual leg muscles during the long jump take-off would help to improve training methods aimed at maximizing jump performance.

## METHODS

Nine experienced long jumpers (4 males, 5 females; age 19.1±1.5 years; mass 57.4±6.1 kg; height 171± 8 cm) volunteered to participate in this study. The study was approved by the Institutional Review Board of Fu Jen Catholic University and each participant gave written informed consent prior to data collection. All jumps were performed in an indoor track-and-field facility and were unaided by wind. A maximum run-up distance of 12 m was available prior to take-off. After landing on the take-off board during the final stride, the participant jumped as far as possible into a sandpit. Each participant performed three trials, and the longest jump was selected for further analysis. Approximately 4-5 minutes of rest time was provided between each trial to minimize fatigue.

Forty-seven reflective markers were placed on prescribed bony landmarks located on 14 body segments, including the head, trunk, upper arm, forearm, thigh, shank, and foot segments (12). An infrared motion capture system sampling at 250 Hz (Motion Analysis, Rohnert Park, CA,

USA) was used to measure the three-dimensional positions of the markers for the duration of the take-off phase, while the corresponding ground reaction force (GRF) was measured simultaneously using a force plate sampling at 2,000 Hz (AMTI, Watertown, WA, USA). The force plate was placed at the take-off location with the front edge of the plate aligned with a foul line marked on the ground. In the present study, a fair jump was determined by the take-off foot landing behind the foul line, and jump performance was taken as the distance measured from the toes of the take-off foot to the rear-most point of the body at landing. The force-plate data were filtered using a third-order Butterworth IIR low-pass filter with a cut-off frequency of 50 Hz. Joint angles were estimated from the measured marker positions by implementing an inverse kinematics algorithm available in OpenSim 3.3, and these data were then filtered using a third-order IIR low-pass filter with a cut-off frequency of 15 Hz. Muscle electromyographic (EMG) data were recorded from a subset of three subjects using a wireless EMG system (DELSYS Inc., Natick, MA, USA) sampling at 1,962 Hz. EMG data were recorded from six muscles of the take-off leg: gluteus medius, soleus, medial gastrocnemius, vastus medialis, rectus femoris, and semitendinosus. The muscle EMG data were filtered using a fourth-order Butterworth high-pass filter with a cut-off frequency of 20 Hz, and subsequently full-wave rectified and filtered using a fourth-order Butterworth low-pass filter with a cut-off frequency of 8 Hz. A high-pass filter was used to remove noise from the raw EMG signal caused by sensor motion artifact (13). Full-wave rectification and low-pass filtering were then used to produce a linear envelope of the EMG signal (14). The processed EMG data were normalized by the peak EMG activity recorded for one complete trial of the long jump encompassing the run-up, approach, take-off and flight phases. All experimental data were extracted to cover the entire take-off phase as well as a pre-contact period equivalent to 30% of the take-off phase. The early, middle, late, and terminal portions of the take-off phase were defined as 0-20%, 20-60%, 60-80%, and 80-100% of ground contact time, respectively.

Participant-specific computer simulations of the take-off phase of the long jump were generated based on a generic model of the body (15). The skeleton was represented as a 29 degree-of-freedom (DOF) articulated linkage, with the pelvis represented as a 6-dof rigid body. The shoulder and hip joints were each modeled as a ball-and-socket joint whereas the elbow, knee, ankle, and metatarsophalangeal (MTP) joints were each represented as a hinge. The ipsilateral take-off leg (i.e., the leg in contact with the ground during the take-off phase) was actuated by 40 muscle-tendon units while the MTP joint (16), contralateral swing leg, and arms were driven by ideal torques. Each musculotendon unit was modeled as a Hill-type muscle in series with an elastic tendon (17). Peak isometric muscle force, $F_O^M$, was calculated using the muscle volume data reported by Miller et al. (18) and assuming a muscle specific tension (i.e., muscle force divided by muscle physiological cross-sectional area) of 60 N/cm$^2$ (19). Muscle activation dynamics was assumed to be first-order (20) with activation and deactivation time constants of 0.01 and 0.04, respectively (21). Six Hunt-Crossley contact spheres were used to model the interaction of the take-off leg with the ground (22): four spheres were placed under the hindfoot segment and two spheres under the toes segment. The static and dynamic frictional coefficients were assumed to be 0.9 and 0.3 respectively, for all contact spheres.

Participant-specific musculoskeletal models were created using a built-in scaling algorithm available in OpenSim 3.3. Segment-specific scaling factors were found by comparing the distance between virtual markers defined in the generic model and corresponding marker positions measured on each participant. These scaling factors were used to scale the segment lengths, segment inertial properties, and muscle attachment sites for each participant. An inverse kinematics analysis then was performed to calculate the joint angles by minimizing the differences between the measured marker positions and the positions of the virtual markers assigned to the model. Participant-specific simulations were generated by solving a dynamic optimization problem to track the joint angles and GRFs measured during the take-off phase.

The dynamic optimization problem was solved by discretizing each state (i.e., joint angles, joint angular velocities, muscle forces, and muscle activations) into 100 evenly-spaced nodes (23, 24). Values of the states at each node were found by minimizing the sum of all muscle activations as well as the differences between the model-predicted and measured joint angles and GRFs. The dynamic optimization solution was computed using a modified version of the direct collocation algorithm developed by Lin and Pandy (23) (see Supplementary Digital Content 1, which presents details relating to the dynamic optimization problem for the long jump take-off and the initial guess used to compute the optimization solution). All simulations were performed in OpenSim (v 3.3) and MATLAB (R2020a).

A pseudo-inverse force decomposition method (25) was used to calculate the contribution of each muscle force to the GRF generated during the take-off phase. At each time step of the simulation, individual muscle contributions to the GRF were found by solving an optimization problem that minimized the induced accelerations of the ground contact spheres subject to the dynamical equations of motion (26). Individual muscle contributions to the vertical and fore-aft GRF impulses were found by integrating each muscle's contribution to the GRF over the duration of the take-off phase. These results were then normalized by body mass to obtain each muscle's contribution to the change in velocity of the COM during take-off.

## RESULTS

Descriptive data for the best long jump recorded for each participant are given in Table 1. Model-predicted joint angles, motion of the whole-body COM, and GRFs were in good agreement with corresponding measurements obtained from experiment (Figs 1 and 2) (see also Supplementary Digital Content 2, which presents a comparison of model-predicted and experimental results for joint angles). Root mean square (RMS) errors for pelvic translations and rotations were $\leq$ 2 cm and $\leq 1^{o}$, respectively. Measured hip, knee, and ankle joint angles

were also accurately tracked with RMS errors of ≤ 3.5°. RMS errors in the model-predicted GRFs were 0.12 BW, 0.14 BW, and 0.11 BW in the fore-aft, vertical, and mediolateral directions, respectively. The simulated positions and velocities of the COM were also closely similar to corresponding experimental data.

The sequence and timing of model-predicted muscle activations were consistent with measured EMG data, albeit with some differences evident (Fig. 3). Perhaps most notably, model-predicted activations for the ankle plantarflexors, GAS and SOL, were higher than the levels of EMG activity recorded for these muscles during terminal swing, whereas model-predicted activations for the quadriceps (VAS and RF) and hamstrings (HAMS) were lower than measured EMG at this time.

VAS developed the highest peak force of all the muscles, followed by SOL and GMAX (Fig. 4). VAS developed a peak force of 12.5 BW (~8000 N) at 40% of ground contact time, as the knee approached maximum flexion (Fig. 4, VAS). The peak force in SOL was 6.0 BW, which occurred at 60% of ground contact time when the ankle reached maximum dorsiflexion (Fig. 4, SOL). GMAX, a uniarticular hip extensor, was activated shortly after touchdown and developed a peak force of 5.5 BW during the initial foot-ground impact (Fig. 4). ILPSO, a uniarticular hip flexor, was activated much later and developed a peak force of 4.7 BW just before the body left the ground. GAS developed a peak force of 3.0 BW, which was much lower than the peak force in SOL and occurred closer to take-off. The force in HAMS remained relatively constant throughout the take-off phase and varied between 2.0 BW and 3.0 BW.

Model-predicted sagittal-plane net moments developed about the hip, knee and ankle joints were consistent with corresponding measurements obtained from inverse dynamics (Fig. 5A). The mean net hip-extensor moment peaked at 5.2 Nm/kg whereas the mean net knee-extensor and ankle-plantarflexor moments peaked at slightly lower magnitudes of 4.5 Nm/kg and 3.6

Nm/kg, respectively. GMAX generated the bulk of the net hip extensor moment throughout the take-off phase, with HAMS contributing substantially (Fig. 5B). ILPSO generated a flexor moment at the hip that increased prior to take-off in preparation for the subsequent flight phase (see Supplementary Digital Content 2, which presents the time history of hip flexion during take-off). VAS generated most of the net extensor moment at the knee whereas HAMS generated a flexor moment that slowed knee extension and prevented the knee from hyperextending at take-off. SOL generated a large fraction of the net ankle-plantarflexor moment, but GAS also contributed appreciably, especially near take-off where its contribution grew to exceed that of SOL (Fig. 5B).

The contributions of the individual muscles of the ipsilateral (take-off) leg to the vertical and fore-aft GRFs revealed a proximal-to-distal sequence of muscle coordination during take-off (Fig. 6). The hip extensor (GMAX), with assistance from the hip abductors (GMED and GMIN) and hip adductor (ADD), were the major contributors during early stance (0-20% ground contact time); the knee extensors (VAS) dominated in midstance (40-60%); the ankle plantarflexors (SOL and GAS) contributed most significantly during late stance (75-90%); and the metatarsal joint was dominant immediately before take-off (90-100%).

GMAX, VAS and SOL were the major contributors to the vertical (support) GRF (Fig. 6A and B, top). GMAX and VAS generated peak support forces of 2.15 BW and 2.60 BW during early and mid-stance, respectively, while SOL generated a peak support force of 2.19 BW in late stance. GAS also contributed appreciably to support and generated a peak force of 0.95 BW just prior to lift-off.

GMAX, VAS and SOL also contributed most significantly to the fore-aft GRF (Fig. 6A and B, bottom). VAS induced the highest braking force, with a peak of 1.43 BW compared to peak braking forces of 0.6 BW and 0.5 BW generated by GMAX and SOL, respectively. The hip

extensors, GMAX and HAMS, also contributed significantly to propulsion, with HAMS generating a propulsive force for the entire take-off phase (Fig. 6A, bottom).

The torques actuating the joints of the contralateral (swing) leg and the arms contributed relatively little to the vertical and fore-aft components of the GRF (Fig. 6C, Swing Leg and Arms; see also Supplementary Digital Content 3, which presents the time histories of the torques applied at the joints of the swing leg, back, and arms). The contribution from all gravitational forces was also comparatively small (Fig. 6C, Gravity). The inertial forces (Coriolis and centrifugal forces) contributed significantly during the initial foot-ground impact whereas the MTP joint contributed markedly just before lift-off (Fig. 6C, Inertia and MTP).

Most muscles delivered a positive vertical (support) impulse that increased the vertical velocity of the COM during take-off (Fig. 7A and B). VAS generated the largest support impulse and increased the vertical COM velocity by 1.8 m/s, which accounted for one-third (33%) of the increase in vertical COM velocity generated by all the muscles. SOL and GMAX generated smaller support impulses and increased the vertical COM velocity by 1.3 m/s and 0.8 m/s, respectively, accounting for 24% and 16% of the increase in vertical COM velocity generated by all the muscles. HAMS and ILPSO (not shown) generated small downward impulses that reduced the vertical COM velocity during take-off.

The muscles of the take-off leg also delivered positive fore-aft (propulsive) and negative fore-aft (braking) impulses that either increased or reduced the forward velocity of the COM (Fig. 7A and B). VAS generated the highest braking impulse and contributed most significantly to a loss in forward COM velocity (Fig. 7A, right panel). VAS reduced the forward COM velocity by 0.92 m/s, which accounted for approximately one-half (55%) of the loss in forward COM velocity generated by all the muscles. The hip and ankle muscles delivered much smaller braking impulses. The ankle plantarflexors, SOL and GAS, generated braking impulses during

the first half of the take-off phase and reduced the forward COM velocity by 0.20 m/s and 0.06 m/s, respectively (Fig. 7A, right panel). SOL contributed 12% while GAS contributed just 4% of the loss in forward COM velocity generated by all the muscles (Fig. 7B). GMAX generated a braking impulse immediately after touchdown and reduced the forward COM velocity by 0.1 m/s, which represented 7% of the loss in forward COM velocity generated by all the muscles.

HAMS delivered the largest propulsive impulse and increased the forward COM velocity by 0.17 m/s, which accounted for 30% of the increase in forward COM velocity generated by all the muscles (Figs 7A and B). HAMS was the only muscle that delivered a propulsive impulse throughout the take-off phase, with no braking effect. The ankle plantarflexors also delivered propulsive impulses during the second half of the take-off phase: SOL and GAS increased the forward COM velocity by 0.09 m/s and 0.12 m/s and accounted for 15% and 20% of the increase in forward COM velocity generated by all the muscles, respectively.

Overall, the net increase in vertical COM velocity generated by all the forces acting on the body during the take-off phase, including gravity and inertia, was 3.3 m/s, whereas the net loss in forward COM velocity was 1.1 m/s (Fig. 7C). The knee extensors (VAS and RF) generated the largest support impulse and increased the vertical COM velocity by 1.9 m/s, while the ankle plantarflexors (SOL and GAS) and hip extensors (GMAX, GMED, ADD and HAMS) increased the vertical COM velocity by 1.6 m/s and 1.2 m/s, respectively. Gravity and inertia generated substantial downward impulses, which reduced the vertical COM velocity by 1.1 m/s and 0.5 m/s, respectively. The knee extensors, primarily VAS, generated the largest braking impulse and contributed most of the loss in forward COM velocity (1.0 m/s), while the ankle plantarflexors and hip extensors made much smaller contributions to slowing the forward velocity of the COM (0.25 m/s and 0.1 m/s, respectively). The hip extensors and ankle plantarflexors also delivered the largest propulsive impulses and increased the forward COM velocity by 0.25 m/s and 0.20 m/s, respectively.

## DISCUSSION

A key determinant of long jump performance is the ability to increase the vertical velocity of the COM while minimizing the loss in forward velocity (running speed) during the take-off phase. We found that the uniarticular hip, knee and ankle extensors dominated the change in COM velocity during take-off. VAS, SOL and GMAX combined to increase the vertical COM velocity by 3.9 m/s, which accounted for 73% of the increase in vertical COM velocity generated by all the muscles (Figs 7A and B). VAS generated the highest support impulse and contributed one-third (33%) of the increase in vertical COM velocity generated by all the muscles. SOL and GMAX also generated substantial support impulses and contributed 24% and 16%, respectively, of the increase in vertical COM velocity. The net increase in the vertical COM velocity was 3.3 m/s, less than the increase in vertical COM velocity due to VAS, SOL and GMAX combined (Fig. 7C). The difference is explained by the actions of gravity and inertia, which generated negative support impulses, accelerated the COM downwards, and reduced the vertical COM velocity at take-off.

While increasing the vertical COM velocity, VAS, SOL, and to a lesser extent, GMAX, also reduced the forward velocity of the COM during take-off (Figs 7A and B). VAS generated the highest braking impulse and contributed approximately one-half (55%) of the loss in forward COM velocity generated by all the muscles. SOL delivered a substantial braking impulse during the first half of the take-off phase and contributed 12% of the loss in forward COM velocity, whereas GMAX generated a braking impulse immediately after touchdown and contributed 7% of the loss in forward COM velocity. Altogether, the lower-limb muscles reduced forward COM velocity by 1.5 m/s, which was greater than the net loss of 1.1 m/s in forward COM velocity (Fig. 7C). The difference is explained by the fact that most muscles also generated a propulsive impulse that increased the forward COM velocity during certain periods of the take-off phase. For example, HAMS delivered a propulsive impulse throughout the take-

314 off phase which accounted for 30% of the increase in forward COM velocity generated by all
315 the muscles (Figs 7A and B).

316 Why is an increase in vertical COM velocity accompanied by a loss in forward COM velocity
317 during take-off? Upward velocity of the COM is generated at the expense of forward velocity
318 because the body pivots about a stationary foot as the stance leg compresses during the first
319 half of the take-off phase (4, 6, 8). Dapena and Chung (8) used a simple kinematic model of
320 the take-off phase of the high jump to show that vertical COM velocity increases after
321 touchdown even though the COM moves radially toward the fixed foot due to flexion of the
322 stance-leg joints. They explained that radial motion of the COM increases the vertical velocity
323 of the COM because the leg muscles experience faster eccentric contractions, allowing them
324 to develop higher forces and generate a higher peak vertical GRF (8). Similar to the behavior
325 described by Dapena and Chung (8) for the high jump, in the long jump take-off vertical
326 velocity of the COM increases shortly after touchdown while the COM moves radially toward
327 the fixed foot (see Supplementary Digital Content 4, which presents the trajectories of the
328 position and velocity of the COM in the vertical and radial directions). A negative radial
329 velocity of the COM (directed toward the foot) is converted to an upward vertical velocity by
330 eccentric (lengthening) contractions of the extensor muscles as they are stretched to resist
331 compression of the stance leg during the first half of the take-off. Our model simulation results
332 showed that the uniarticular hip extensor, GMAX, lengthened immediately after touchdown,
333 developed a peak force of 5.5 BW (Fig. 4, GMAX), and contributed significantly to the first
334 peak in the vertical GRF (Fig. 6A). As the knee and ankle joints then flexed for the remainder
335 of the first half of the take-off phase, VAS and SOL lengthened appreciably, developed peak
336 forces of 12.5 BW and 5.5 BW respectively (Fig. 4, VAS and SOL), and contributed
337 significantly to the second peak in the vertical GRF (Fig. 6B) (see Supplementary Digital
338 Content 4, which presents the lengths and velocities of the muscle fibers computed for the

uniarticular hip, knee and ankle extensors during take-off). The vertical velocity of the COM continued to increase upward during the second half of the take-off phase as GMAX, VAS and SOL all underwent concentric contractions (shortening) until lift-off.

Maximizing forward COM velocity (running speed) during the approach phase is an important feature of the long jump (1, 2). Not unexpectedly then, there are similarities in how the lower-limb muscles are used to maximize performance in steady-speed sprinting and the long jump take-off. In both of these activities the combined actions of VAS and the ankle plantarflexors, SOL and GAS, contribute a large fraction of the support impulse generated at each step (27). Further, in both steady-state sprinting and the long jump take-off, VAS contributes practically all the braking impulse generated on the ground (27). However, one major difference between the two activities is that the net fore-aft impulse during steady-speed sprinting is nearly zero whereas during the long jump take-off the net braking impulse is substantial with a magnitude >1.0 N.s/kg. The reason the net fore-aft impulse remains close to zero in steady-speed sprinting is because the ankle plantarflexors, SOL and GAS, generate large propulsive impulses which overcome the braking action of VAS (27). The ankle plantarflexors also generate propulsive impulses in the second half of the long jump take-off, however their total contribution to the net fore-aft impulse during take-off is much smaller than that in sprinting, which explains why the net fore-aft impulse during the long jump take-off is dominated by the braking action of VAS. Another key difference between steady-speed sprinting and the long jump take-off is the contribution made by the hip muscles to the support impulse. In steady-state sprinting, the hip muscles, GMAX, GMED and ADD, contribute relatively little to the support impulse generated at each step (27), whereas these muscles each make a notable contribution to the support impulse generated during the long jump take-off (Figs 6A and 7A).

The ability to generate vertical velocity during take-off is a critical determinant of long jump performance. We found that VAS contributes most significantly to the vertical velocity of the

364 COM at take-off (Fig. 7), implying that coaches and athletic trainers ought to focus foremost
365 on strengthening the quadriceps muscles if performance of the long jump is to be improved.
366 Our simulation results also show that the hip and ankle extensors play a major role in generating
367 an upward velocity of the COM during take-off (Fig. 6). GMAX produced most of the support
368 impulse generated during impact immediately after touchdown, whereas SOL contributed a
369 large fraction of the support impulse generated during the second half of the take-off phase
370 (Figs 6 and 7). Thus, GMAX and SOL also should be targeted in strength training programs
371 aimed at maximizing jump performance. It should be noted that increasing the volumes of these
372 muscles would also alter the inertial properties of the limbs (specifically the masses and
373 locations of the centers of mass of the thigh and shank segments) and may negatively impact
374 jump performance by increasing body mass and/or altering muscle coordination during the run-
375 up. Addressing this issue quantitatively requires a predictive modelling approach, like the
376 dynamic optimization technique used recently by Lin and Pandy (28) who investigated the
377 effects of changes in muscle strength and other muscle-tendon properties on sprint performance.

378 Perhaps the most significant limitation of the present study was the limited run-up distance
379 available to our jumpers, which most likely explains the shorter jump distances recorded by
380 our athletes compared to data reported by others (3-6). Run-up distances used in official
381 competitions are typically 40 m, allowing the athlete to complete around 14 strides before
382 reaching the board (29). By comparison, the maximum run-up distance available in the present
383 study was just 12 m, which would have limited approach velocity and hence jump distance
384 appreciably. Lees and colleagues measured long jump performance in elite female (6) and male
385 (4) collegiate athletes. They reported mean jump distances of 6.51 m for women and 7.67 m
386 for men. At touchdown, the mean forward and vertical velocities were reported to be 8.75 m/s
387 and -0.03 m/s, respectively, for women, compared to mean forward and vertical velocities of
388 9.88 m/s and -0.15 m/s for men. At take-off, the mean forward and vertical velocities were 7.55

m/s and 3.05 m/s, respectively, for women, compared to mean forward and vertical velocities of 8.75 m/s and 3.01 m/s for men. The mean jump distance for our cohort of male and female Taiwanese athletes was much lower at 5.18 m, with corresponding mean forward and vertical velocities at touchdown of 7.65 m/s and -0.58 m/s, respectively, and mean forward and vertical velocities at take-off of 6.65 m/s and 2.67 m/s, respectively. Nonetheless, the change in position and velocity of the COM from touchdown to take-off measured for our athletes closely resembled the data published by Lees and colleagues (4, 6). For both men and women, these authors found the vertical position of the COM to dip slightly just after touchdown and then to increase sharply after maximum knee flexion until take-off. We also found a slight dip in the vertical position of the COM immediately after touchdown as the velocity of the COM was directed downwards (Fig. 1). The vertical velocity of the COM then increased sharply before declining just before take-off, consistent with the trend noted by Lees et al. (4, 6). Another limitation of the present study concerns the structure of the model used to simulate the long jump take-off. Whereas the joints of the ipsilateral (take-off) leg were actuated by muscles, the joints of the contralateral (swing) leg, arms and torso were driven by ideal torques. We simplified the musculoskeletal model in this way because the mechanics of the take-off leg is known to contribute more substantially to the vertical velocity of the COM generated during take-off than either the swing leg or the arms (4). Indeed, we found that the torques actuating the joints of the contralateral leg and arms contributed little to the vertical and fore-aft components of the GRF (Fig. 6C). However, this does not mean that the arms and contralateral leg are not important contributors to performance of the long jump. Swinging the contralateral leg and arms during the take-off phase serves to transfer angular momentum to the whole body prior to lift-off, which promotes an efficient landing (30). Future studies should examine how muscle actuation of the swing leg and arms affect take-off biomechanics and jump distance. Finally, we simulated only the take-off phase of the long jump and ignored the preceding strides

where the forward approach velocity is known to peak (3). Future work should consider expanding the analysis presented here to include the last 2 to 3 strides in addition to the take-off phase to better understand how the leg muscles maximize long jump performance.

In summary, the uniarticular hip, knee and ankle extensors dominated the change in COM velocity during the long-jump take-off. VAS, SOL, and GMAX contributed nearly three-quarters (73%) of the increase in the vertical velocity of the COM at take-off, with VAS and SOL contributing more than one-half (57%) of the total increase in vertical velocity. VAS also delivered the highest braking impulse and contributed more than one-half (55%) of the reduction in forward velocity of the COM during take-off. These results suggest that the hip, knee and ankle extensors ought to be prioritized in strength training programs aimed at improving long jump performance.

## ACKNOWLEDGEMENTS

This work was supported in part by a Discovery Projects Grant from the Australian Research Council (DP160104366) awarded to MGP. A Postgraduate Research Scholarship provided to KY by the University of Melbourne is also gratefully acknowledged. We thank Dr Yi-Chung Lin for his advice related to model development.

## CONFLICT OF INTEREST STATEMENT

The authors declare no competing or financial interests. The results of the present study do not constitute endorsement by the American College of Sports Medicine and are presented clearly, honestly, and without fabrication, falsification, or inappropriate data manipulation.

435 REFERENCES

436 1. Hay JG. The biomechanics of the long jump. Exerc Sport Sci Rev. 1986;14(1):401-
437 46.
438 2. Alexander RM. Optimum take-off techniques for high and long jumps. Philos Trans R
439 Soc Lond B Biol Sci. 1990;329(1252):3-10.
440 3. Hay JG, Miller JA, Canterna RW. The techniques of elite male long jumpers. J
441 Biomech. 1986;19(10):855-66.
442 4. Lees A, Graham-Smith P, Fowler N. A biomechanical analysis of the last stride,
443 touchdown, and takeoff characteristics of the men's long jump. J Appl Biomech.
444 1994;10(1):61-78.
445 5. Graham-Smith P, Lees A. A three-dimensional kinematic analysis of the long jump
446 take-off. J Sports Sci. 2005;23(9):891-903.
447 6. Lees A, Fowler N, Derby D. A biomechanical analysis of the last stride, touch-down
448 and take-off characteristics of the women's long jump. J Sports Sci. 1993;11(4):303-14.
449 7. Luhtanen P, Komi PV. Mechanical power and segmental contribution to force
450 impulses in long jump take-off. Eur J Appl Physiol Occup Physiol. 1979;41(4):267-74.
451 8. Dapena J, Chung CJM. Vertical and radial motions of the body during the take-off
452 phase of high jumping. Med Sci Sports Exerc. 1988;20(3):290-302.
453 9. Seyfarth A, Friedrichs A, Wank V, Blickhan R. Dynamics of the long jump. J
454 Biomech. 1999;32(12):1259-67.
455 10. Seyfarth A, Blickhan R, Van Leeuwen JL. Optimum take-off techniques and muscle
456 design for long jump. J Exp Biol. 2000;203(4):741-50.
457 11. Kakihana W, Suzuki S. The EMG activity and mechanics of the running jump as a
458 function of takeoff angle. J Electromyogr Kinesiol. 2001;11(5):365-72.

12. Cappozzo A, Cappello A, Croce UD, Pensalfini F. Surface-marker cluster design criteria for 3-D bone movement reconstruction. IEEE Trans Biomed Eng. 1997;44(12):1165-74.

13. De Luca CJ. The use of surface electromyography in biomechanics. J Appl Biomech. 1997;13(2):135-63.

14. Lai A, Schache AG, Brown NA, Pandy MG. Human ankle plantar flexor muscle–tendon mechanics and energetics during maximum acceleration sprinting. J R Soc Interface. 2016;13(121).

15. Lai AKM, Arnold AS, Wakeling JM. Why are antagonist muscles co-activated in my simulation? A musculoskeletal model for analysing human locomotor tasks. Ann Biomed Eng. 2017;45(12):2762-74.

16. Chen W-M, Shim VP-W, Park S-B, Lee T. An instrumented tissue tester for measuring soft tissue property under the metatarsal heads in relation to metatarsophalangeal joint angle. J Biomech. 2011;44(9):1801-4.

17. De Groote F, Kinney AL, Rao AV, Fregly BJ. Evaluation of direct collocation optimal control problem formulations for solving the muscle redundancy problem. Ann Biomed Eng. 2016;44(10):2922-36.

18. Miller R, Balshaw TG, Massey GJ, Maeo S, Lanza MB, Johnston M, et al. The muscle morphology of elite sprint running. Med Sci Sports Exerc. 2020;53(4):804-15.

19. Rajagopal A, Dembia CL, DeMers MS, Delp DD, Hicks JL, Delp SL. Full-body musculoskeletal model for muscle-driven simulation of human gait. IEEE Trans Biomed Eng. 2016;63(10):2068-79.

20. Zajac FE. Muscle and tendon: properties, models, scaling, and application to biomechanics and motor control. Crit Rev Biomed Eng. 1989;17(4):359-411.

21. Winters JM, Stark L. Estimated mechanical properties of synergistic muscles involved in movements of a variety of human joints. J Biomech. 1988;21(12):1027-41.

22. Sherman MA, Seth A, Delp SL. Simbody: multibody dynamics for biomedical research. Procedia Iutam. 2011;2(1):241-61.

23. Lin Y-C, Pandy MG. Three-dimensional data-tracking dynamic optimization simulations of human locomotion generated by direct collocation. J Biomech. 2017;59(1):1-8.

24. Lin Y-C, Walter JP, Pandy MG. Predictive simulations of neuromuscular coordination and joint-contact loading in human gait. Ann Biomed Eng. 2018;46(8):1216-27.

25. Lin YC, Kim HJ, Pandy MG. A computationally efficient method for assessing muscle function during human locomotion. Int J Numer Method Biomed Eng. 2011;27(3):436-49.

26. Anderson FC, Pandy MG. Individual muscle contributions to support in normal walking. Gait Posture. 2003;17(2):159-69.

27. Pandy MG, Lai AKM, Schache AG, Lin YC. How muscles maximize performance in accelerated sprinting. Scand J Med Sci Sports. 2021;31(10):1882-96.

28. Lin Y-C, Pandy MG. Predictive Simulations of Human Sprinting: Effects of Muscle-Tendon Properties on Sprint Performance. Med Sci Sports Exerc. 2022.

29. Bridgett LA, Linthorne NP. Changes in long jump take-off technique with increasing run-up speed. J Sports Sci. 2006;24(8):889-97.

30. Bouchouras G, Moscha D, Papaiakovou G, Nikodelis T, Kollias I. Angular momentum and landing efficiency in the long jump. Eur J Sport Sci. 2009;9(1):53-9.

506 **FIGURE CAPTIONS**

507 Fig. 1: Time histories of model-predicted vertical and fore-aft displacements and velocities
508 (red lines) of the center of mass (COM) of the body during the take-off phase of the
509 long jump. The blue lines are the mean of the experimental data recorded for the
510 participants. The shaded regions represent $\pm$ 1 standard deviation from the mean for
511 both the model and experimental data. 0% and 100% of ground contact time represent
512 touchdown and take-off, respectively. The origin (0,0) of the coordinate system used
513 to measure COM position was located at the upper left corner of the force plate
514 embedded in the ground.

515 Fig. 2: Time histories of model-predicted vertical, fore-aft, and mediolateral components of
516 the ground reaction force (GRF) (red lines) generated during the take-off phase of the
517 long jump. The blue lines are the mean of the experimental data recorded for the
518 participants, The shaded regions represent $\pm$ 1 standard deviation from the mean for
519 both the model and experimental data. 0% and 100% of ground contact time represent
520 touchdown and take-off, respectively. BW, body weight.

521 Fig. 3: Comparison of model-predicted activations (red) and measured EMG activity (blue)
522 for selected muscles crossing the hip, knee and ankle joints. Shaded regions depict $\pm$
523 1 standard deviation from the mean. EMG data were measured from 3 of the 9
524 participants and then averaged across participants. EMG data for each muscle were
525 normalized by the peak value recorded during the take-off phase. Muscle symbols are:
526 GASMED: medial gastrocnemius; GMED: anterior portion of gluteus medius; RF:
527 rectus femoris; SEMITEN: semitendinosus; SOL: soleus; VASMED: vastus medialis.
528 0% and 100% of ground contact time represent touchdown and take-off, respectively.

529 Fig. 4: Time histories of the forces calculated in representative muscles during the take-off
530 phase of the long jump. The solid lines are mean muscle forces calculated for all

participants and the shaded regions represent ± 1 standard deviation from the mean. Muscle forces were normalized by each participant's body weight (BW). Muscle symbols are: GMAX, superior, middle, inferior portions of gluteus maximus combined; RF, rectus femoris; GMED, anterior and posterior portions of gluteus medius combined; HAMS, semimembranosus, semitendinosus, and biceps femoris long head and short head combined; ILPSO, iliacus and psoas combined; VAS, vastus medialis, intermedius, and lateralis combined; SOL, soleus; GAS, medial and lateral gastrocnemius combined. 0% and 100% of ground contact time represent touchdown and take-off, respectively.

Fig. 5: (A) Time histories of the net moments developed by all the muscles spanning the hip, knee, and ankle joints during the take-off phase of the long jump. Moments were normalized by each participant's body mass and averaged across all participants. The shaded regions represent ± 1 standard deviation from the mean. Hip extension, knee extension and ankle plantarflexion are positive. 0% and 100% of ground contact time represent touchdown and take-off, respectively.

(B) Contributions of individual muscles to the net joint moments exerted about the hip, knee, and ankle during the take-off phase. Muscle moments were normalized by each participant's body mass and averaged across all participants. Hip extension, knee extension and ankle plantarflexion are positive. Muscle symbols are defined in Fig. 4. 0% and 100% of ground contact time represent touchdown and take-off, respectively.

Fig. 6: Mean contributions of the hip-spanning muscles (A), knee- and ankle-spanning muscles (B), and gravity, inertia, swing leg, arms, and metatarsal joint (C) to the vertical and fore-aft ground reaction forces generated during the take-off phase of the long jump. The light black dashed lines represent the total GRF induced by the ipsilateral (take-off) leg. The blue shaded regions are the measured vertical and fore-

aft GRFs averaged across all participants. 0% and 100% of ground contact time represent touchdown and take-off, respectively. Muscle symbols are: GMAX, superior, middle, inferior portions of gluteus maximus combined; GMED, anterior and posterior portions of gluteus medius combined; GMIN, anterior and posterior portion of the gluteus minimus; RF, rectus femoris; ADD, adductor brevis, adductor longus and adductor magnus combined. HAMS, semimembranosus, semitendinosus, and biceps femoris long head and short head combined; VAS, vastus medialis, intermedius, and lateralis combined; SOL: soleus; GAS, medial and lateral gastrocnemius combined; OTHER, summed contributions from all other muscles included in the model. Other symbols appearing in the diagram are: MTP, metatarsophalangeal joint torque applied to the take-off leg; Swing leg, combined joint torques applied to the contralateral (swing) leg; Arms, combined joint torques applied to the left and right arms; Gravity, sum of all gravitational forces acting on the body; Inertial, sum of all velocity-related forces including Coriolis and centrifugal forces, applied to the body.

Fig. 7: (A) Mean contributions of selected muscles to the change in COM velocity during the take-off phase of the long jump. Positive values represent upward- and forward-directed velocities while negative values represent downward- and backward-directed velocities. (A) Contributions of individual muscles to the change in vertical COM velocity (left panel) and forward COM velocity (right panel). (B) Percentage contributions of individual muscles to the change in the vertical and forward velocities of the COM. 100% represents the contribution made by all muscles in the model to the change in the vertical and forward velocity of the COM. (C) Mean contributions of the hip extensors (GMAX, GMED, ADD and HAMS), knee extensors (VAS and RF), ankle plantarflexors (SOL and GAS), metatarsophalangeal (MTP) joint,

contralateral (swing) leg, arms, gravity, and inertial forces to the change in vertical and forward COM velocity during the take-off phase of the jump. Symbols are defined in Fig. 6.

## Supplementary Digital Content

Supplementary Digital Content 1.docx

Supplementary Digital Content 2.docx

Supplementary Digital Content 3.docx

Supplementary Digital Content 4.docx

# Muscle Contributions to Take-off Velocity in the Long Jump
# SUPPLEMENTARY DIGITAL CONTENT 1

## Dynamic Optimization Problem for the Long Jump Take-off

Kaiwen Yang[1], Wen-Tzu Tang[2], Shu-Hua Liu[2,3], Marcus G. Pandy[1]

[1]Dept of Mechanical Engineering, University of Melbourne, Parkville, Victoria, Australia

[2]Graduate Institute of Athletics and Coaching Science, National Taiwan Sport University, Taoyuan City, Taiwan

[3]Physical Education Office, Ming Chuan University, Taoyuan City, Taiwan

### Dynamic optimization problem

The data-tracking optimal control problem was converted into a nonlinear optimization problem by discretizing the model states into 100 evenly spaced nodes (1, 2). Values of the joint angles ($q$), joint angular velocities ($u$), muscle-tendon forces ($F$), muscle activations ($a$), and ideal torques ($\tau$) applied at the torque-driven joints at each node, along with the values of a subset of the time-invariant Hunt-Crossley contact parameters (specifically, height of the contact plane, dissipation constant and viscous friction coefficient) were found by minimizing the performance criterion $J$:

$$J = J_q + J_{GRF} + J_{GRM} + J_{ID} + J_a + J_\tau \quad (1)$$

Here $J_q$ minimizes the integral sum of the differences between model-predicted and measured joint angles with a weighting factor of $10^4$; $J_{GRF}$ and $J_{GRM}$ respectively minimize the integral sum of the differences between model-predicted and measured ground reaction forces and moments with

weighting factors of $10^5$ and $10^3$; $J_{ID}$ minimizes the integral sum of the differences between model-predicted and measured joint torques for the take-off leg (specifically, hip extension, adduction, knee extension, and ankle plantarflexion torque) with a weighting factor of $10^3$; and $J_a$ and $J_\tau$ minimize respectively the integral sum of muscle activations squared and joint torques squared with weighting factors of 1 and $10^2$.

The data-tracking dynamic optimization problem was solved subject to a trapezoidal state defect constraint (1) at each node, thus:

where x is the vector of model states comprised of the generalized coordinates, generalized speeds, muscle activations, and muscle fiber lengths ($l_m$); n is the node number; and t is time.

**Initial guess for dynamic optimization solution**

To obtain better tracking performance, an initial guess for the optimization solution was generated using a two-step procedure. In Step 1, an optimization-based inverse dynamics problem was solved using ideal joint torques to track the measured joint coordinates. The simulated time history of the joint motion closely tracked the measured data while maintaining dynamical consistency (3). The 6-dimensional pelvis residual forces and torques were minimized as pelvic motion was not explicitly generated by muscles.

Step 1 involved calculating the variables $(q, u, \tau)$ needed to minimize the objective function:

$$w_q(q - q_{EXP})^T(q - q_{EXP}) + \frac{1}{2}\tau^T H\tau \tag{3}$$

subject to the constraints

$$u_{i+1} = u_i + \frac{1}{2}\Delta t\ (q_i + q_{i+1}) \tag{4}$$

$$a_{i+1} = a_i + \frac{1}{2}\Delta t\ (u_i + u_{i+1}) \tag{5}$$

where $w_q = 100$ is the weighting factor applied to the coordinate tracking term in the objective function, and $H$ is a square diagonal weighting matrix with dimension equal to the number of model DOFs. For the pelvis residual torque, a higher weighting factor of 10 was used to minimize the pelvic residuals while a lower weighting factor of 0.1 was used for the remaining joint torques to ensure the model tracked the movement path with minimal effort. In equation (5) above, $a$ is a vector of joint accelerations and was computed using explicit dynamics based on the dynamical equations of motion:

$$a = M(q)^{-1}(F_{inertial}(q,u) + F_{GRF} + F_{gravity} + \tau) \tag{6}$$

Step 1 converged to a solution within 10-20 mins with a cluster of 6 CPUs in parallel.

In the Step 2, the joint torques $\tau$ obtained in the Step 1 were decomposed into individual muscle forces by solving a static optimization problem at each time step along the movement trajectory. Specifically, Step 2 involved calculating the muscle activations $a$ and the ideal torques $\tau_q$ needed to minimize the quadratic objective function:

$$a^T a + w\ \tau_q^T \tau_q \tag{7}$$

subject to the linear constraints

$$\tau = \tau_q + MA(FV \cdot FL \cdot \cos(\alpha)\, a) \tag{8}$$

with bounds

$$a \in [0,1] \tag{9}$$

where $w$ is a weighting factor whose value was taken to be 1000. A large weighting factor was used to penalize the residual torques in the muscle-actuated joints. Also, $\alpha$ was a vector of muscle pennation angles, and FV and FL were vectors containing multipliers used to specify each muscle's force-length and force-velocity properties. FV, FL and $\alpha$ were derived assuming a rigid tendon for each musculotendon unit included in the model. Step 2 solved very efficiently in less than 5 seconds because the optimization problem was posed as a quadratic programming problem.

The time histories of the joint angles ($q$) and joint angular velocities ($u$) obtained in Step 1 were amalgamated with the time histories of the muscle activations ($a$) and muscle forces ($F$) obtained in Step 2 to form the initial guess for the dynamic optimization problem for the long jump take-off.

**Optimizer Settings**

The optimization was solved using the MATLAB built-in solver "fmincon" (MathWorks, Natick, MA, USA). The optimization algorithm used was 'interior-point' and the 'SubproblemAlgorithm' selected was 'cg', which is the abbreviation for the conjugate gradient algorithm. The optimization algorithm was previously developed and verified by Byrd et al. (4).

The Jacobian of the constraint function and the gradient of the objective function were provided to the solver. The multibody dynamics state derivatives with respect to the skeletal states and generalized forces were estimated using finite differences while the derivatives of the muscle states with respect to the muscle states and muscle length were derived analytically using symbolic operation. Since the muscle length and muscle moment arm with respect to the joint angles were trained using smooth polynomials, the derivatives of the constraint functions with respect to all optimization design variables could be derived using the derivative chain rule. The Hessian matrix was estimated using the built-in option 'bfgs'.

Finally, the termination step length tolerance (StepTolerance) was 1e-6; the constraint tolerance (ConstraintTolerance) was 1e-2; and the first-order optimality tolerance (OptimalityTolerance) was 1e-5. Each optimization program took between 1.5 hours and 4 hours to converge on a 6-core, 32GB RAM desktop with an Intel i9 processor.

# REFERENCES

1. Lin Y-C, Pandy MG. Three-dimensional data-tracking dynamic optimization simulations of human locomotion generated by direct collocation. *J Biomech.* 2017;59(1):1-8.

2. Lin Y-C, Walter JP, Pandy MG. Predictive simulations of neuromuscular coordination and joint-contact loading in human gait. *Ann Biomed Eng.* 2018;46(8):1216-27.

3. Runge C, Zajac F, Allum J, Risher D, Bryson A, Honegger F. Estimating net joint torques from kinesiological data using optimal linear system theory. *IEEE Trans Biomed Eng.* 1995;42(12):1158-64.

4. Byrd RH, Hribar ME, Nocedal J. An interior point algorithm for large-scale nonlinear programming. *SIAM J Optim.* 1999;9(4):877-900.

# Muscle Contributions to Take-off Velocity in the Long Jump

# SUPPLEMENTARY DIGITAL CONTENT 3

## Model-computed Joint Torques During the Long-jump Take-off

Kaiwen Yang[1], Wen-Tzu Tang[2], Shu-Hua Liu[2,3], Marcus G. Pandy[1]

[1]Dept of Mechanical Engineering, University of Melbourne, Parkville, Victoria, Australia

[2]Graduate Institute of Athletics and Coaching Science, National Taiwan Sport University, Taoyuan City, Taiwan

[3]Physical Education Office, Ming Chuan University, Taoyuan City, Taiwan

Below we present plots of the histories of model-predicted joint torques (black lines), ideal joint torques (red lines), and muscle-generated joint torques (green lines) calculated in the model for participant #1 during the take-off phase of the long jump. Participant #1 used her right leg as the takeoff leg. 0% and 100% of ground contact time represent touchdown and take-off, respectively.

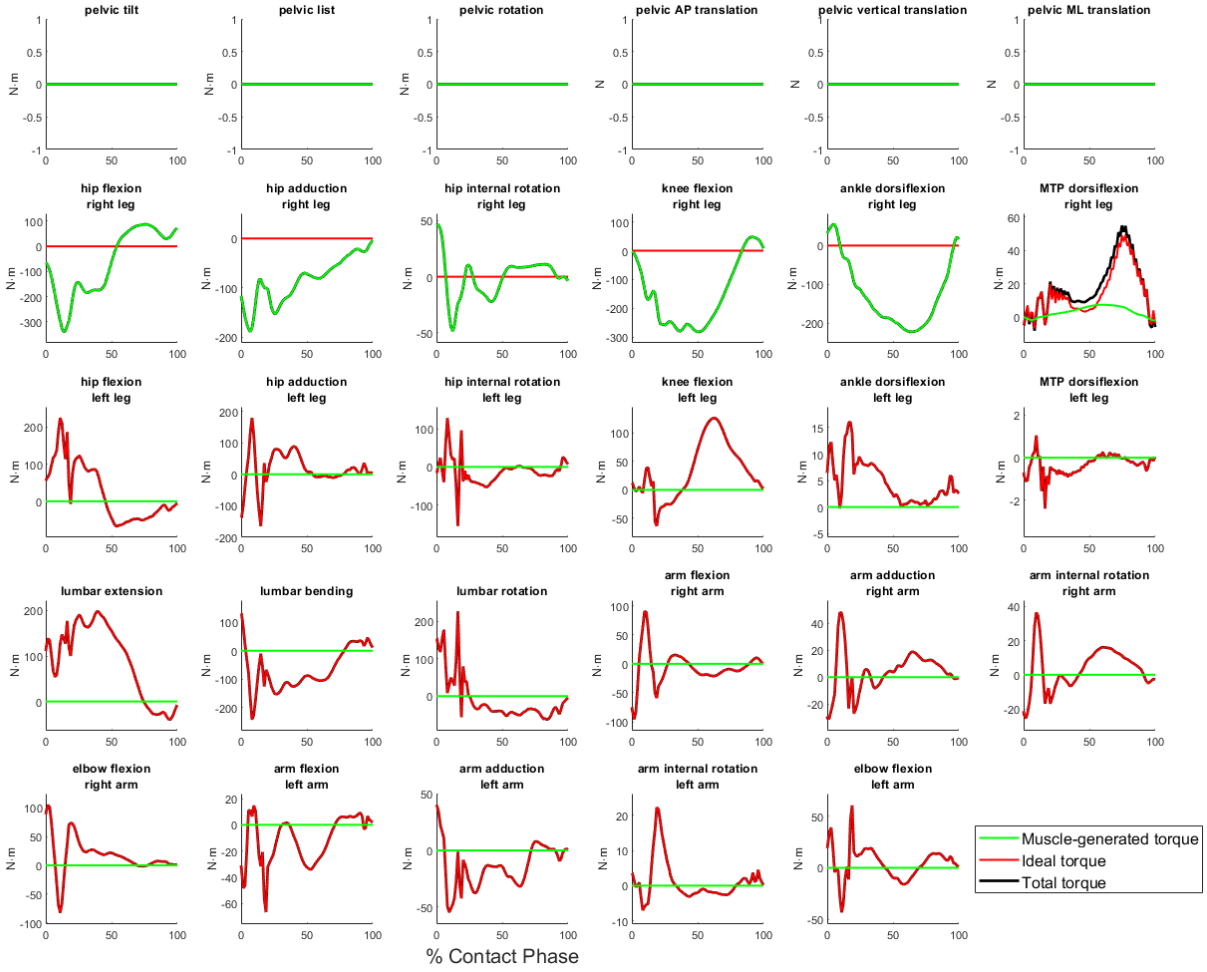
pelvic tilt
pelvic list
pelvic rotation
pelvic AP translation
pelvic vertical translation
pelvic ML translation
hip flexion right leg
hip adduction right leg
hip internal rotation right leg
knee flexion right leg
ankle dorsiflexion right leg
MTP dorsiflexion right leg
hip flexion left leg
hip adduction left leg
hip internal rotation left leg
knee flexion left leg
ankle dorsiflexion left leg
MTP dorsiflexion left leg
lumbar extension
lumbar bending
lumbar rotation
arm flexion right arm
arm adduction right arm
arm internal rotation right arm
elbow flexion right arm
arm flexion left arm
arm adduction left arm
arm internal rotation left arm
elbow flexion left arm
N·m
N
% Contact Phase
Muscle-generated torque
Ideal torque
Total torque

# Muscle Contributions to Take-off Velocity in the Long Jump
# SUPPLEMENTARY DIGITAL CONTENT 2

## Model-predicted Joint Motion

Kaiwen Yang[1], Wen-Tzu Tang[2] , Shu-Hua Liu[2,3], Marcus G. Pandy[1]

[1]Dept of Mechanical Engineering, University of Melbourne, Parkville, Victoria, Australia

[2]Graduate Institute of Athletics and Coaching Science, National Taiwan Sport University, Taoyuan City, Taiwan

[3]Physical Education Office, Ming Chuan University, Taoyuan City, Taiwan

Below we present plots of the time histories of model-predicted joint motion (red lines) during the take-off phase of the long jump. Data for the hip, knee, and ankle joint angles are for the take-off leg. The blue lines are the mean of the experimental data recorded for the participants while the shaded regions represent $\pm$ 1 standard deviation from the mean. 0% and 100% of ground contact time represent touchdown and take-off, respectively.

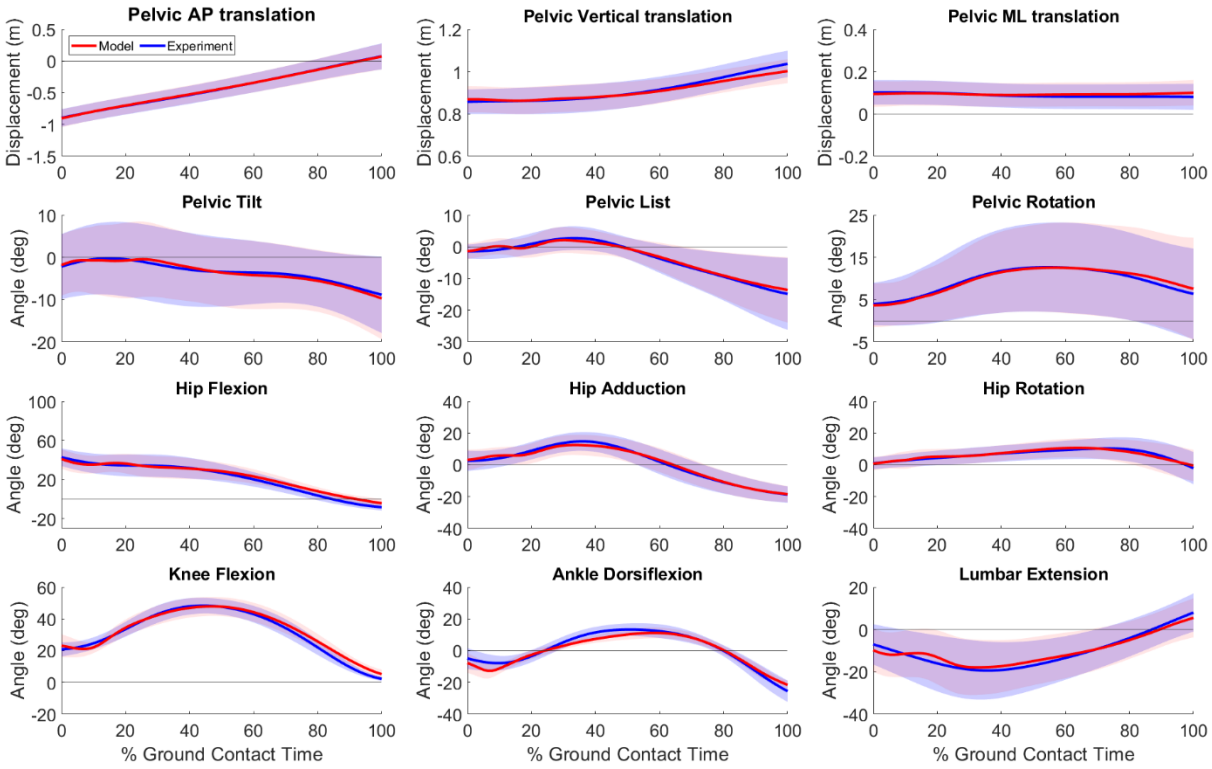
Pelvic AP translation
Model
Experiment
Displacement (m)
Pelvic Vertical translation
Displacement (m)
Pelvic ML translation
Displacement (m)
Pelvic Tilt
Angle (deg)
Pelvic List
Angle (deg)
Pelvic Rotation
Angle (deg)
Hip Flexion
Angle (deg)
Hip Adduction
Angle (deg)
Hip Rotation
Angle (deg)
Knee Flexion
Angle (deg)
Ankle Dorsiflexion
Angle (deg)
Lumbar Extension
Angle (deg)
% Ground Contact Time
% Ground Contact Time
% Ground Contact Time

# Muscle Contributions to Take-off Velocity in the Long Jump

# SUPPLEMENTARY DIGITAL CONTENT 4

## Kinematics of the Mass Center and Lower-limb Joints and Muscles

Kaiwen Yang[1], Wen-Tzu Tang[2], Shu-Hua Liu[2,3], Marcus G. Pandy[1]

[1]Dept of Mechanical Engineering, University of Melbourne, Parkville, Victoria, Australia

[2]Graduate Institute of Athletics and Coaching Science, National Taiwan Sport University, Taoyuan City, Taiwan

[3]Physical Education Office, Ming Chuan University, Taoyuan City, Taiwan

Below we present plots of the position and velocity of the center of mass of the whole body during the take-off phase of the long jump (Figure S4.1) followed by plots of the time histories of muscle-fiber lengths and velocities computed during the take-off phase (Figure S4.2). Also shown in Figure S4.2 are the angular displacements and velocities of the hip, knee, and ankle joints calculated in the model during the take-off phase.

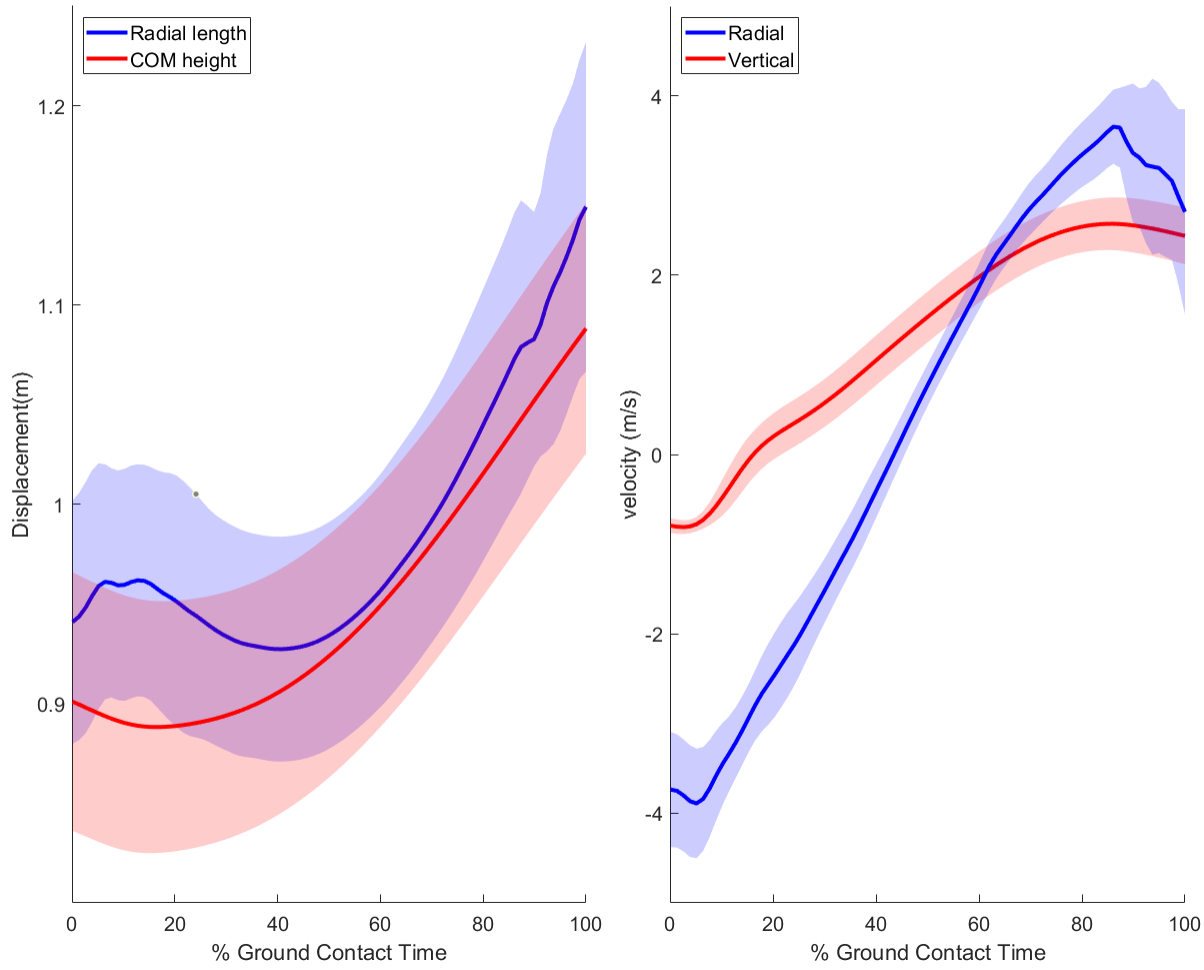


Figure S4.1: Left Panel: Radial (blue line) and vertical (red line) displacement of the center of mass over the contact phase.

Right Panel: Radial (blue line) and vertical (red line) velocity of the center of mass over the contact phase. The solid lines are the mean of the model-predicted results for the participants, and the shaded regions represent $\pm$ 1 standard deviation from the mean. 0% and 100% of ground contact time represent touchdown and take-off, respectively.

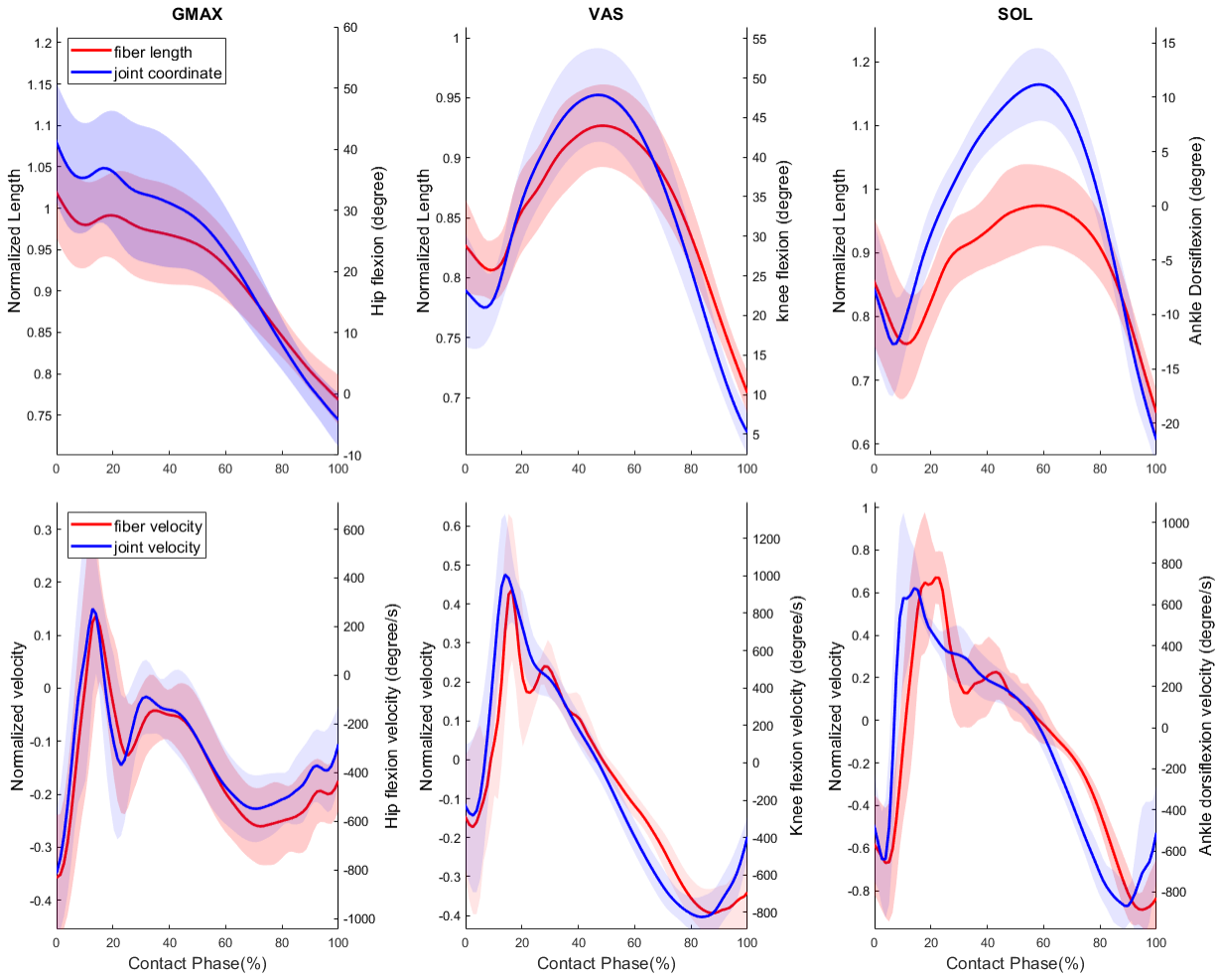


Figure S4.2: GMAX, VAS, and SOL fiber kinematics. First row: Fiber lengths computed for GMAX, VAS, and SOL normalized by their corresponding optimal muscle-fiber lengths (red lines). Also plotted on the same set of axes are the angular displacements of the hip, knee and ankle joints (blue lines). The solid lines are the mean of the model-predicted joint angles and joint angular velocities calculated across all participants, and the shaded regions represent $\pm$ 1 standard deviation from the mean. 0% and 100% of ground contact time represent touchdown and take-off, respectively.

Second row: Velocities of the muscle fibers computed for GMAX, VAS, and SOL normalized by their corresponding maximum shortening velocities (red lines). Also plotted on the same set of axes are the angular velocities of the hip, knee and ankle joints (blue lines). The solid lines are the mean of the model-predicted muscle-fiber lengths, muscle-fiber velocities, and joint kinematics calculated across all participants, and the shaded regions represent $\pm$ 1 standard deviation from the mean. 0% and 100% of ground contact time represent touchdown and take-off, respectively. Muscle symbols are: GMAX, superior, middle, inferior portions of gluteus maximus combined; VAS, vastus medialis, intermedius, and lateralis combined; SOL, soleus.

Table 1: Physical characteristics of study participants and spatiotemporal data recorded for each participant's longest jump. Year-best Performance: Longest jump recorded for each participant in 2020; Touchdown Leg Angle: Angle measured in the sagittal plane between the ground and the line connecting the COM of the body and the center of pressure acting under the take-off foot at the instant of touchdown (i.e., 0% of the stance phase); Takeoff Angle: Angle measured in the sagittal plane between the resultant velocity of the COM of the body and the ground. Jump Distance was defined as the distance measured from the last point of contact of the foot immediately before take-off to the rearmost mark in the sandpit upon landing. s.d., standard deviation.

| Participant | Mass (kg) | Gender | Height (cm) | Age (yrs) | Take-off Leg | Year-Best Performance (m) | Approach Velocity | | Takeoff Velocity | | Touchdown Leg Angle (deg) | Takeoff Angle (deg) | Ground Contact Time(sec) | Jump Distance (m) |
|---|---|---|---|---|---|---|---|---|---|---|---|---|---|---|
| | | | | | | | Fore-aft (m/s) | Vertical (m/s) | Fore-aft (m/s) | Vertical (m/s) | | | | |
| 1 | 62 | F | 170 | 22 | R | 6.06 | 7.366 | -0.729 | 5.913 | 2.906 | 59.07 | 26.17 | 0.145 | 5.34 |
| 2 | 60 | M | 180 | 20 | R | 6.50 | 8.046 | -0.459 | 7.357 | 2.492 | 60.90 | 18.71 | 0.152 | 6.23 |
| 3 | 54 | F | 169 | 19 | L | 5.92 | 7.570 | -0.602 | 6.738 | 2.408 | 62.01 | 19.67 | 0.143 | 5.36 |
| 4 | 60 | M | 180 | 20 | R | 6.50 | 8.111 | -0.630 | 7.171 | 2.726 | 62.50 | 20.81 | 0.151 | 6.04 |
| 5 | 44 | F | 159 | 20 | R | 5.91 | 6.867 | -0.576 | 5.779 | 2.924 | 61.31 | 26.84 | 0.136 | 4.92 |
| 6 | 59 | F | 172 | 18 | R | 5.20 | 6.637 | -0.612 | 6.168 | 2.130 | 67.97 | 19.05 | 0.138 | 4.62 |
| 7 | 54 | F | 158 | 18 | R | 5.32 | 6.817 | -0.638 | 5.680 | 2.591 | 60.75 | 24.52 | 0.136 | 4.53 |
| 8 | 59 | M | 173 | 17 | L | 6.69 | 8.333 | -0.561 | 7.386 | 2.773 | 60.72 | 20.58 | 0.120 | 6.05 |
| 9 | 65 | M | 181 | 18 | L | 7.18 | 9.111 | -0.442 | 7.684 | 3.147 | 58.17 | 22.27 | 0.123 | 6.40 |
| Mean±s.d. | 57.44±6.13 | | 171.3±8.5 | 19.1±1.5 | | 6.14±0.64 | 7.65±0.82 | -0.58±0.09 | 6.65±0.78 | 2.67±0.31 | 61.49±2.78 | 22.07±3.07 | 0.138±0.011 | 5.50±0.71 |